Supporting Information to accompany

DFT prediction and experimental investigation of valence tautomerism in cobalt-dioxolene complexes

Gemma K. Gransbury[†], Marie-Emmanuelle Boulon[‡], Simon Petrie[§], Robert W. Gable[†], Roger J. Mulder[⊥], Lorenzo Sorace[‡], Robert Stranger[§], Colette Boskovic[†]*

*Email: c.boskovic@unimelb.edu.au

[†] School of Chemistry, University of Melbourne, VIC 3010, Australia

[‡] UdR INSTM and Department of Chemistry "U. Schiff", University of Florence, 50019 Sesto Fiorentino (FI), Italy

[§] Research School of Chemistry, College of Physical & Mathematical Sciences, Australian National University, ACT 2601, Australia

[⊥] CSIRO Manufacturing, Clayton, VIC 3168, Australia

Contents:

S.I.-1 Thermogravimetric Analysis

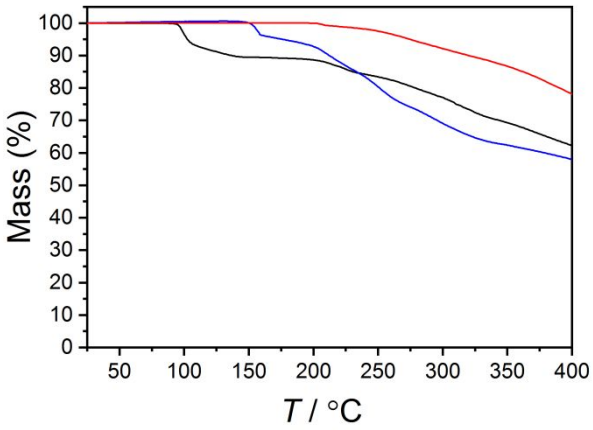

Figure S1. Thermogravimetric analysis of **1** (red), **1(PF$_6$)**·1.2tol (black) and **1(BPh$_4$)** (blue).

S.I.-2 Infrared Spectroscopy

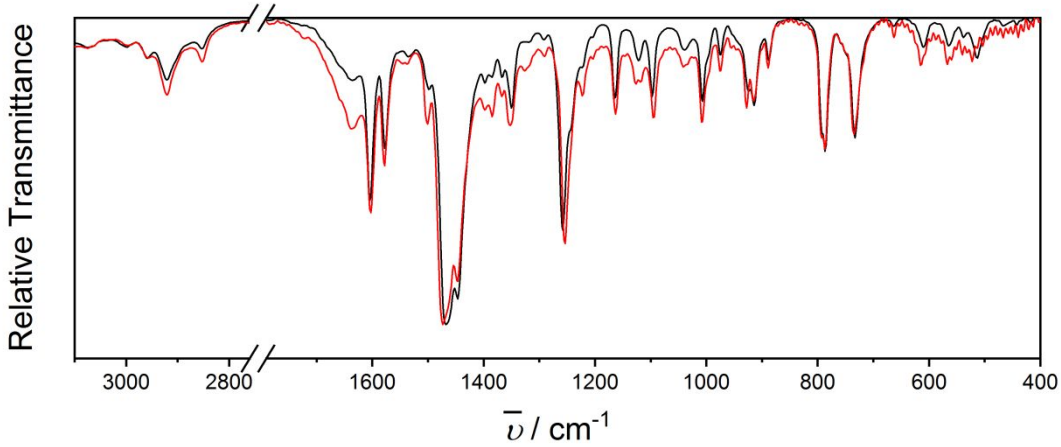

Figure S2. Infrared spectra of **1** (black) and **1-Zn** (red)

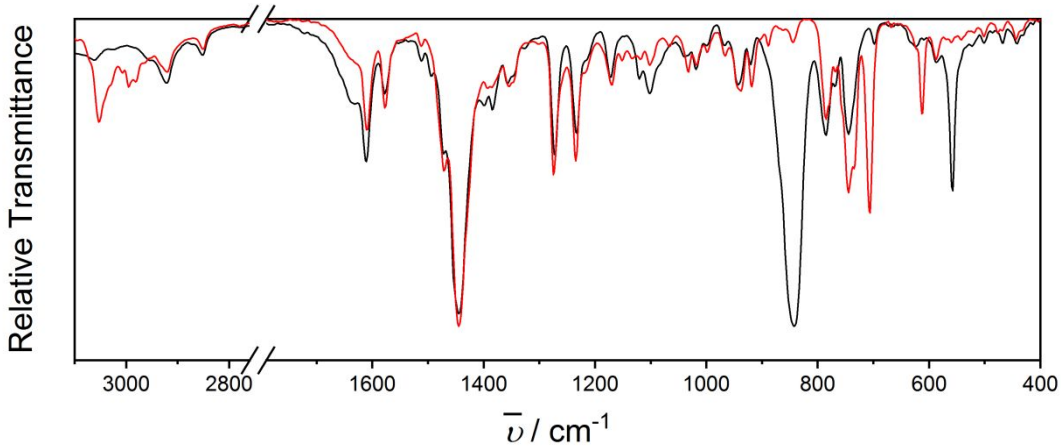

Figure S3. Infrared spectra of **1(PF$_6$)**·1.2tol (black) and **1(BPh$_4$)** (red).

S.I.-3 Crystallographic Study

S.I.-3a Crystallographic Data

Table S1. Crystallographic data for compound **1**, **1-Zn** and **1(BPh$_4$)**

	1	**1-Zn**	**1(BPh$_4$)**
formula	$C_{27}H_{24}Br_4CoN_4O_2$	$C_{27}H_{24}Br_4Zn\ N_4O_2$	$C_{51}H_{44}BBr_4CoN_4O_2$
fw/g mol^{-1}	815.07	821.51	1134.28
cryst syst	monoclinic	monoclinic	monoclinic
space group	$P2_1/n$	$P2_1/n$	$P2_1/c$
color	red	yellow	brown
a/Å	11.28581(8)	11.3061(2)	29.677(6)
b/Å	13.55349(10)	13.5329(3)	9.963(2)
c/Å	18.54192(14)	18.5931(4)	30.000(6)
β/deg	92.7048(6)	92.566(2)	96.26(3)
V/Å^3	2833.05(4)	2841.97(10)	8817(3)
Z	4	4	8
T/K	130.01(10)	130.00(10)	100(2)
ρ_{calc}/g cm^{-3}	1.911	1.920	1.709
μ/mm^{-1}	11.626	8.055	4.062
reflns measd	19888	21068	160030
unique reflns	5820	5936	24718
data/restraints/param	5820/0/346	5936/0/346	24718/0/1142
R_{int}	0.0267	0.0433	0.0769
R_1 [$I > 2s(I)$]	0.0227	0.0322	0.0506
wR_2 (all data)	0.0558	0.0886	0.1405
GOF on F^2	1.074	1.027	1.026
$\Delta\rho_{max/min}$/e Å^{-3}	0.40/-0.71	0.44/-0.86	2.34/-1.50

Table S2. Temperature-dependent crystallographic data for compound **1(PF$_6$)**·2tol

	100 K	200 K	250 K	275 K	300 K	315 K	330 K	380 K
formula	$C_{41}H_{40}Br_4CoN_4O_2PF_6$	$C_{41}H_{40}Br_4CoN_4O_2PF_6$	$C_{41}H_{40}Br_4CoN_4O_2PF_6$	$C_{41}H_{40}Br_4CoN_4O_2PF_6$	$C_{41}H_{40}Br_4CoN_4O_2PF_6$	$C_{41}H_{40}Br_4CoN_4O_2PF_6$	$C_{41}H_{40}Br_4CoN_4O_2PF_6$	$C_{41}H_{40}Br_4CoN_4O_2PF_6$
fw/g mol^{-1}	1144.31	1144.31	1144.31	1144.31	1144.31	1144.31	1144.31	1144.31
cryst syst	tetragonal	tetragonal	tetragonal	tetragonal	tetragonal	tetragonal	tetragonal	tetragonal
space group	$P4_2/n$	$P4_2/n$	$P4_2/n$	$P4_2/n$	$P4_2/n$	$P4_2/n$	$P4_2/n$	$P4_2/n$
color	brown	brown	brown	brown	brown	brown	brown	brown
a/Å	24.721(4)	24.861(4)	24.974(4)	25.058(4)	25.059(4)	25.115(4)	25.177(4)	25.232(4)
b/Å	24.721(4)	24.861(4)	24.974(4)	25.058(4)	25.059(4)	25.115(4)	25.177(4)	25.232(4)
c/Å	13.918(3)	13.969(3)	13.987(3)	13.984(3)	14.005(3)	13.997(3)	13.992(3)	14.006(3)
V/Å^3	8506(3)	8634(3)	8724(3)	8781(3)	8794(3)	8828(3)	8870(3)	8917(3)
Z	8	8	8	8	8	8	8	8
T/K	100(2)	200(2)	250(2)	275(2)	300(2)	315(2)	330(2)	380(2)
ρ_{calc}/g cm^{-3}	1.787	1.761	1.743	1.731	1.729	1.722	1.714	1.705
μ/mm^{-1}	4.267	4.204	4.161	4.134	4.127	4.111	4.092	4.070
reflns measd	154547	146282	135350	103798	130926	103338	66624	83631
unique reflns	10184	10344	9501	7198	9112	7237	4598	5867
data/restraints/param	10184/0/579	10344/0/477	9501/6/475	7198/8/470	9112/12/475	7237/2/463	4598/104/456	5867/104/458
R_{int}	0.1045	0.0726	0.0714	0.0752	0.0675	0.0747	0.0834	0.0915
R_1 [$I > 2s(I)$]	0.0386	0.0408	0.0485	0.0570	0.0460	0.0557	0.0721	0.0591
wR_2 (all data)	0.1031	0.1094	0.1393	0.1723	0.1317	0.1707	0.2219	0.1758
GOF on F^2	1.033	1.016	1.036	1.023	1.026	1.029	1.059	1.020
$\Delta\rho_{max/min}$/e Å^{-3}	0.89/-0.61	1.12/-0.67	0.97/-0.58	1.02/-0.63	0.80/-0.63	0.78/-0.69	0.68/-0.63	0.73/-0.76

S.I.-3b Variable temperature bond lengths of 1(PF_6)·2tol

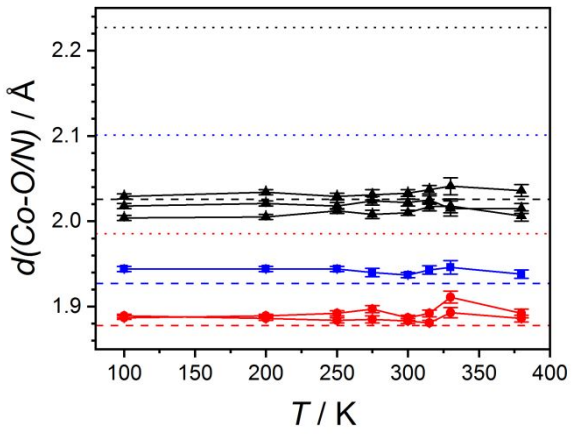

Figure S4. Temperature dependence of Co-O (red), Co-N_{amine} (blue) and Co-N_{py} (black) bond lengths in **1(PF_6)**·2tol from single crystal X-ray crystallography study. Reference lines show average bond lengths for LS Co(III)-cat (dashed) and HS Co(II)-sq (dotted) DFT-optimized structures of $\mathbf{1}^+$.

S.I.-3c Crystal Packing Diagrams

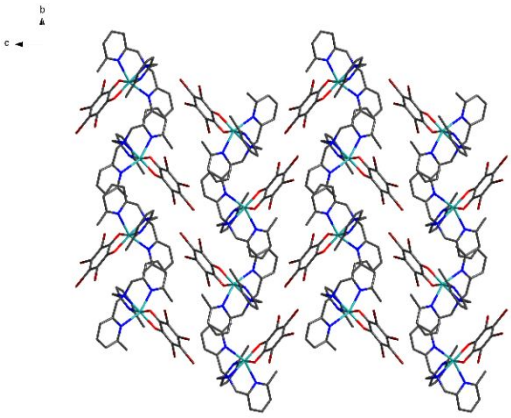

Figure S5. Crystal packing of **1** as viewed along the *a*-axis. Color code: carbon, black; oxygen, red; nitrogen, blue; cobalt, aqua green; bromine, brown. Compound **1-Zn** shows identical packing.

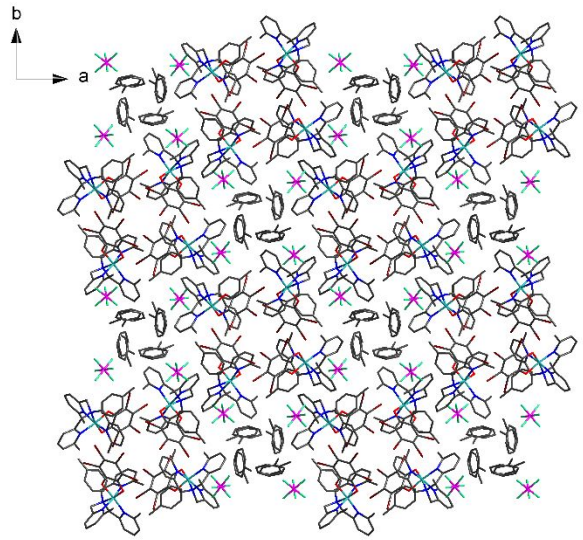

Figure S6. Crystal packing of **1(PF$_6$)**·2tol as viewed along the *c*-axis. Color code: carbon, black; oxygen, red; nitrogen, blue; cobalt, aqua green; phosphorus, magenta; fluorine, bright green.

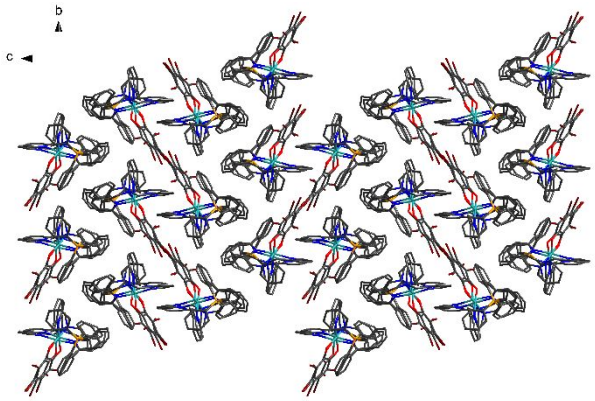

Figure S7. Crystal packing of **1(BPh$_4$)** as viewed along the *a*-axis. Color code: carbon, black; oxygen, red; nitrogen, blue; cobalt, aqua green; boron, orange.

S.I.-4 Powder X-ray Diffraction

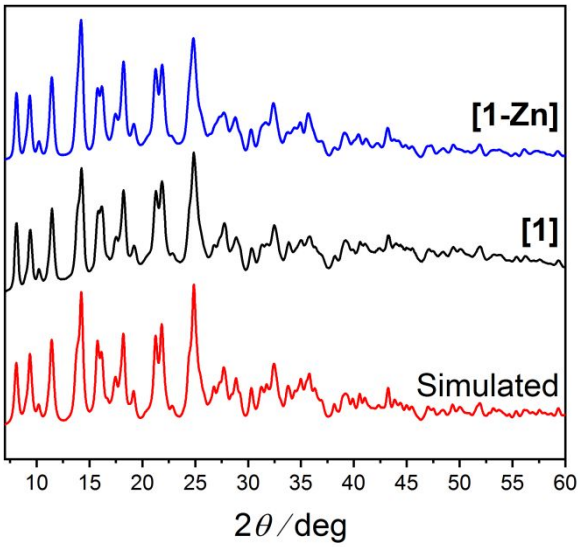

Figure S8. Simulated powder X-ray diffraction patterns of **1** and experimental pattern of **1** and **1-Zn**.

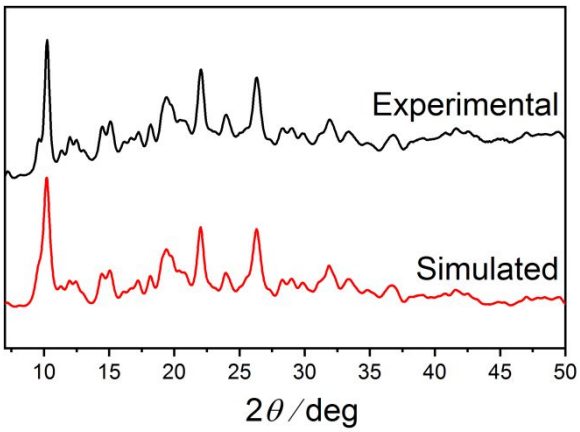

Figure S9. Powder X-ray diffraction pattern of **1(PF_6)**·1.2tol and simulated from the single crystal structure of **1(PF_6)**·2tol.

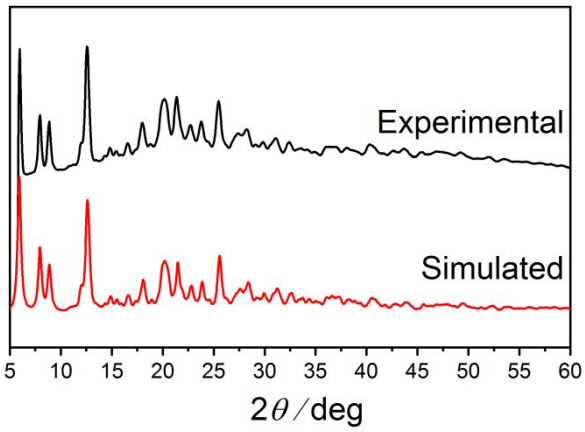

Figure S10. Simulated and experimental powder X-ray diffraction pattern of **1(BPh$_4$)**.

S.I.-5 Variable Temperature UV-Vis

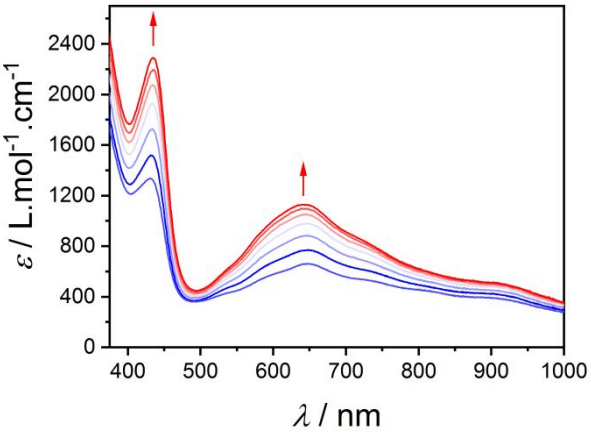

Figure S11. Temperature-dependence of the UV-visible spectrum of **1**$^+$ in DCE from 283 K (blue) to 343 K (red) in 10 K intervals.

S.I.-6 Regular Solution Model Fitting Parameters

Table S3. Minimum and maximum $\chi_M T$ from fitting of Evans method data

Solvent	$(\chi_M T)_{min}$ / cm^3 K mol^{-1}	$(\chi_M T)_{max}$ / cm^3 K mol^{-1}
DCE	0.52 ± 0.02	3.17 ± 0.05
DCM	0.39 ± 0.02	3.17[a]
MeCN	0.22 ± 0.02	3.17[a]

[a] Fixed from DCE results.

S.I-7 VT Thermodynamics

Assuming a valence tautomeric equilibrium:

$$\text{Co(III)-cat} \rightleftharpoons \text{Co(II)-sq} \qquad \text{(S1)}$$

the redox potentials of the one-electron oxidation and reduction processes can be defined as follows.

If Co(III)-cat is the stabilized valence tautomer:

$$\text{Oxidation: Co(III)-cat} \rightleftharpoons \text{Co(III)-sq} + e^-,\ E_{ox} \qquad \text{(S2)}$$

$$\text{Reduction: Co(III)-cat} + e^- \rightleftharpoons \text{Co(II)-cat},\ E_{red} \qquad \text{(S3)}$$

Or, if Co(II)-sq is the stabilized valence tautomer:

Oxidation: Co(II)-sq ⇌ Co(III)-sq + e^-, E_{ox} (S4)

Reduction: Co(II)-sq + e^- ⇌ Co(II)-cat, E_{red} (S5)

Both the oxidation and reduction processes can be observed by electrochemistry for the VT complex. In the case of $\mathbf{1}^+$, the LS-Co(III)-cat valence tautomer is stabilized in DMF solution and therefore Equations (S2) and (S3) are used to define E_{ox} and E_{red}. However, as the oxidation defined in Equation (S2) is irreversible, E_{ox} is estimated by the peak potential measured at a scan rate of 100 mV s^{-1}. We then define:

$$\Delta ox\text{-}red = E_{ox} - E_{red}, \quad \text{(S6)}$$

therefore $\Delta G = -F(\Delta ox\text{-}red)$ corresponds to the Gibbs free energy change of the comproportionation reaction defined by either Equation (S7) or (S8) depending on the VT form present.

Co(II)-cat + Co(III)-sq ⇌ 2 Co(III)-cat (S7)

Co(II)-cat + Co(III)-sq ⇌ 2 Co(II)-sq (S8)

The equations above can be generalized to any VT complex with the following equilibrium:

$$M^m L^l \rightleftharpoons M^{m-1} L^{l+1} \qquad \text{(S9)}$$

Note that $\Delta ox\text{-}red$ differs from quantities used to estimate the ΔG of the VT transition in literature.[1-4] Previous studies used the following two redox processes, of which only one was observed directly for the VT complex, with the other measured for an analogue with a different metal or different dioxolene:

$$\text{Metal-based process: Co(III)-cat} + e^- \rightleftharpoons \text{Co(II)-cat}, \; E_{metal} \qquad \text{(S10)}$$

$$\text{Ligand-based process: Co(II)-sq} + e^- \rightleftharpoons \text{Co(II)-cat}, \; E_{ligand} \qquad \text{(S11)}$$

The difference in potential of (S10) and (S11) relates to the Gibbs free energy change of the VT equilibrium (S1), with $\Delta G = -F(E_{metal} - E_{ligand})$. Note that determining ΔG this way requires either E_{metal} or E_{ligand} to be measured for an analogous complex. Once again, these equations can be generalized to the VT equilibrium (S9).

S.I.8 DFT Calculations on Geometric Isomers of [Co(Me$_n$tpa)(Xdiox)]$^+$

Multiple geometric isomers are possible in the family of [Co(Me$_n$tpa)(Xdiox)]$^+$ complexes. Prior to optimizing the VT transition energies, three ideas were investigated:

(i) is there a Co-dioxolene plane of symmetry present that could be used to speed up calculations?

(ii) which geometric isomer is favoured with the Metpa and Me$_2$tpa ligands?

(iii) what is the preferred orientation of asymmetric dioxolenes?

These questions were answered through a series of gas-phase optimizations of both Co(III)-cat and Co(II)-sq electronic configurations at the BP86/TZP level of theory. No relativistic correction was used in these initial calculations.[5-6]

S.I.-8a Symmetric Dioxolenes

Complexes with [Co(Me$_n$tpa)(Xdiox)]$^+$, n = 0-3 and X = H$_4$, Cl$_4$ were considered in the investigation of *(i)* and *(ii)* (Tables S4 and S5). Two geometries were considered for tpa (n = *0*) complexes: the symmetry-enforced planar structure (C_S) and the bent asymmetric structure (C_1). It was found that Co(III)-cat tpa complexes with X = H$_4$, Cl$_4$ possess a plane of symmetry in the plane of the dioxolene and Co. The same complexes in the Co(II)-sq electronic configuration do not possess any symmetry elements.

In complexes [Co(Me$_3$tpa)(Xdiox)]$^+$, X = H$_4$, Cl$_4$, enforcing a plane of symmetry restricts methyl group rotation. Up to five geometric isomers were considered: the bent asymmetric structure (C_1) and symmetry-enforced planar structures (C_S) with all four combinations of methyl group orientations that obey C_S symmetry. The orientations are described in terms of the methyl groups pointing towards or away from dioxolene side of the

molecule: (i) all towards, (ii) all away, (iii) axial positions towards and equatorial positions away and (iv) axial positions away and equatorial positions towards ("mixed away"). Theoretically (i) and (iv) are interconvertible while maintaining symmetry, as are (ii) and (iii) (see Tables S4 and S5). All (iii) structures were found to convert to the (ii) geometry during the optimization. In Me_3tpa complexes with X = H_4, Cl_4, the C_1 bent geometry was found to be lower in energy than any of the C_S enforced structures in both the Co(III)-cat and Co(II)-sq; bent geometries are consistent with the steric bulk imposed by Me_3tpa.

In complexes of Metpa and Me_2tpa (n = 1, 2), two geometric isomers are possible. Metpa can bind with the Me in the equatorial Co-diox plane (*eq*) or in one of the axial positions (*ax*). Four geometries were compared: the *ax* isomer (symmetry C_1); the *eq* isomer in C_1 symmetry; and the *eq* isomer in C_S symmetry with methyl group pointing towards or away from the dioxolene. The *ax* isomer was found to be lower in energy for all Xdiox ligands, in agreement with the crystal structure of [Co(Metpa)(*t*Bu_2diox)](PF_6)·tol which has 50:50 disorder of Me over the two axial positions (Figure S14).[1] Both *ax* and *eq* isomers of Metpa with octahedral transition metal complexes are common; the less sterically hindered carbonate-based ligands on cobalt favour the Metpa equatorial isomer instead.[7-8]

Similarly, Me_2tpa can bind with Me in the two axial positions (*ax-ax*) or with one axial and one equatorial Me (*ax-eq*). Four geometries were considered: *ax-eq* (C_1); *ax-ax* (C_1); *ax-ax* (C_S with methyl groups pointing towards the dioxolene) and *ax-ax* (C_S with methyl groups pointing away from the dioxolene). All reported cobalt complexes with Me_2tpa exist as *ax-eq* isomers;[7, 9-10] however, the *ax-ax* Me_2tpa isomer has been reported for other metal complexes.[11-19] Calculations on the [Co(Me_2tpa)(Xdiox)]$^+$ complexes indicate the *ax-eq* arrangement of Me groups is favoured, in agreement with the crystal structure of [Co(Me_2tpa)(*t*Bu_2diox)](PF_6)·EtOH (Figure S14).[1]

Table S4. Energies from geometry optimizations of $[Co(Me_ntpa)(Cl_4diox)]^+$ with BP86/TZP theory and a range of symmetry restrictions. Lowest energy isomers of each electromer are indicated in bold.

n	**Isomer**	**Electromer**	**Energy / kJ mol^{-1}**				**Description**
			C_S			**C_1**	
0	N/A	Co(III)-cat	-32112.03			**-32112.08**	planar
		Co(II)-sq	-32021.84			**-32035.82**	bent
			away	*towards*			
1	*eq*	Co(III)-cat	-33672.83	-33671.15		-33673.95	bent
		Co(II)-sq	-33604.04	-33603.73		-33614.63	bent
	ax	Co(III)-cat	N/A			**-33680.55**	planar, ring twisted
		Co(II)-sq				**-33618.88**	bent
			away	*towards*			
2	*ax-ax*	Co(III)-cat	-35235.77	-35235.67		-35236.24	planar, ring twisted
		Co(II)-sq	-35186.92	-35183.85		-35194.24	bent
	ax-eq	Co(III)-cat	N/A			**-35242.40**	bent
		Co(II)-sq				**-35198.53**	bent
			away	*towards*	*mixed away*		
3	N/A	Co(III)-cat	-36785.94	-36791.14	-36791.95	**-36796.38**	bent
		Co(II)-sq	-36763.01	Moved[a]	-36764.58	**-36772.33**	bent

[a] Moved to mixed away arrangement

Table S5. Energies from geometry optimizations of $[Co(Me_ntpa)(H_4diox)]^+$ with BP86/TZP theory and a range of symmetry restrictions. Lowest energy isomers of each electromer are indicated in bold.

n	Isomer	Spin state	Energy / kJ mol^{-1}				Description
			C_S			C_1	
0	N/A	Co(III)-cat	**-32784.62**			-32784.59	planar
		Co(II)-sq	-32702.67			**-32784.58**	bent
			away	*towards*			
1	*eq*	Co(III)-cat	-34344.31	-34342.91		-34345.84	bent
		Co(II)-sq	-34283.72	-34283.49		-34294.02	bent
	ax	Co(III)-cat	N/A			**-34353.47**	bent
		Co(II)-sq				**-34298.85**	bent
			away	*towards*			
2	*ax-ax*	Co(III)-cat	-35907.92	-35909.26		-35910.52	bent
		Co(II)-sq	-35867.63	-35864.62		-35874.83	bent
	ax-eq	Co(III)-cat	N/A			**-35914.84**	bent
		Co(II)-sq				**-35878.41**	bent
			away	*towards*	*mixed away*		
3	N/A	Co(III)-cat	-37458.58	-37463.92	-37463.8	**-37468.95**	bent
		Co(II)-sq	-37443.35	-37445.26	-37445.32	**-37452.70**	very bent

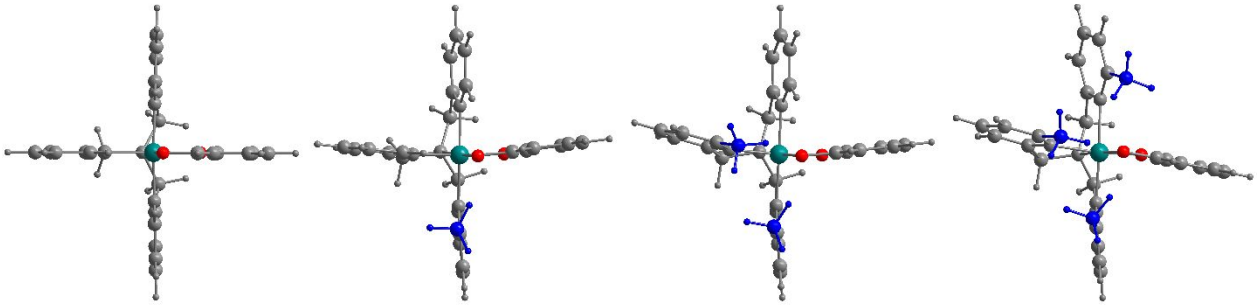

Figure S12. Calculated geometries of $[Co(Me_ntpa)(H_4diox)]^+$ in the Co(III)-cat state with BP86/TZP theory. Cobalt in green, oxygen atoms in red, methyl groups indicated in blue.

Calculations indicated that complexes with symmetric dioxolenes Cl_4diox and H_4diox have a plane of symmetry for $n = 0$ in the Co(III)-cat state, but as *n* increases the complexes

become more distorted and are reduced to C_1 symmetry. A twisting of the axial pyridine rings and a bending of the equatorial pyridine ring out of the dioxolene plane is observed (see Figure S12). Complexes with Metpa complexes favoured the *ax* isomer, while Me_2tpa complexes favoured the *ax-eq* isomer. Calculations for the prediction of new complexes $[Co(Me_ntpa)(Br_4diox)]^+$ were restricted to these isomers and C_1 symmetry for n = 1, 2, 3 (see Table S6).

Table S6. Energies from optimizations of $[Co(Me_ntpa)(Br_4diox)]^+$ using BP86/TZP theory. Lowest energy isomers of each electromer are indicated in bold.

	Energy / kJ mol^{-1}				
Spin state	***n* = 0**		***n* = 1**	***n* = 2**	***n* = 3**
	C_S	**C_1**	**C_1**	**C_1**	**C_1**
Co(III)-cat	**-31863.79**	-31863.04	**-33432.11**	**-34993.77**	**-36548.07**
Co(II)-sq	-31770.70	**-31783.54**	**-33366.63**	**-34946.85**	**-36520.36**

S.I.-8b Asymmetric Dioxolenes: *t*Bu_2diox

Complexes of asymmetric dioxolenes such as $[Co(Me_ntpa)(Xdiox)]^+$, n = 0-3 and X = 3,5-Me_2, 3,5-*t*Bu_2 introduce one further degree of isomerisation: O1 can be *trans* or *cis* to the tertiary amine nitrogen. Although it is commonplace to replace *t*Bu groups with Me groups or H in computational methodology, this is inaccurate for the prediction of VT as the greater electron withdrawing properties of *t*Bu affect the redox properties of the dioxolene.[20] Large *t*Bu groups have significant barriers to rotation and may not optimize to the global minimum in a geometry optimization; however, obtaining the lowest energy conformation of the *t*Bu groups is important as it is of the same order of magnitude as the VT transition energy.

The *t*Bu_2diox geometry was investigated with $[Co(Me_ntpa)(tBu_2diox)]^+$ with n = 0, 3. The barriers to *t*Bu rotation were significant and so three staggered *t*Bu orientations for each

trans and *cis* isomer were considered (see Figure S13) and their energies compared (sees Table S7 and S8). Calculations were undertaken for both spin states: Co(III)-cat and Co(II)-sq.

Assumptions were made to reduce the number of calculations. Based on the results for symmetric dioxolenes above, both C_S and C_1 symmetries were used for tpa complexes, but only C_1 symmetries for Me_3tpa complexes. Calculations were performed on C_1 isomers first ($n = 0$) and if the *t*Bu orientation was significantly higher in energy, the C_S geometry was not considered for this orientation – this resulted in (c), (d) and (f) geometries being excluded for some C_S structures.

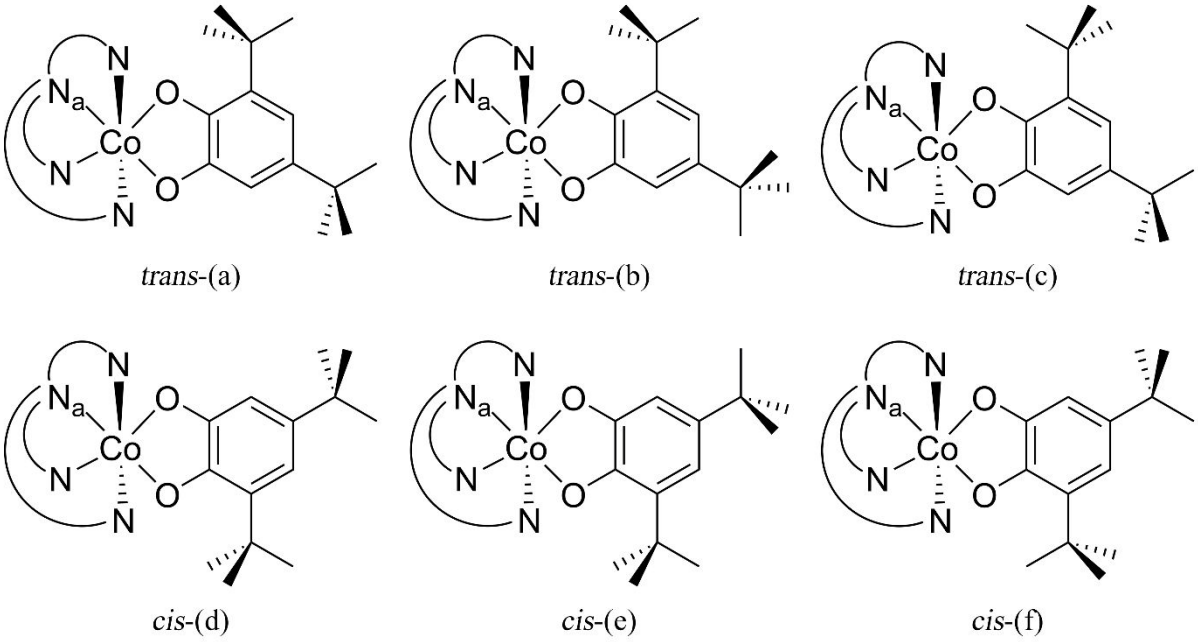

Figure S13. Potential *t*Bu orientations in $[Co(Me_ntpa)(tBu_2cat)]^+$. N_a represents N_{amine}.

Table S7. Energies of geometry optimizations of $[Co(tpa)(tBu_2diox)]^+$ with *t*Bu orientations as described in Figure S13 and BP86/TZP theory. Lowest energy isomers of each electromer are indicated in bold.

		Energy / kJ mol^{-1}					
		trans			*cis*		
Spin state	**Symmetry**	**(a)**	**(b)**	**(c)**	**(d)**	**(e)**	**(f)**
Co(III)-cat	C_S	-45290.97	-45291.41			-45311.91	
	C_1	-45313.84	**-45314.24**	-45302.25	-45311.92	-45312.30	-45300.12
Co(II)-sq	C_S	-45241.67	-45245.14			-45244.40	
	C_1	-45255.90	**-45258.54**	-45242.21	-45252.28	-45255.55	-45238.89

Table S8. Energies of geometry optimizations of $[Co(Me_3tpa)(tBu_2diox)]^+$ with tBu orientations as described in Figure S13 and BP86/TZP theory. Lowest energy isomers of each electromer are indicated in bold.

	Energy (kJmol^{-1})					
	trans			*cis*		
Spin state	**(a)**	**(b)**	**(c)**	**(d)**	**(e)**	**(f)**
Co(III)-cat	**-49999.75**	Dissoc.[a]	DNC[b]	-49994.93[a]	-49997.86[a]	-49982.08[a]
Co(II)-sq	-49991.62	**-49994.54**	-49978.77	-49982.13	-49985.41	-49973.47

[a] Complex began to dissociate due to steric hindrance of *t*Bu and Me_3tpa in Co(III)-cat state
[b] Calculation did not converge.

Calculations indicated that *trans*-(b) orientation of *t*Bu groups was favoured (Table S7 and S8). Rotation of the *t*Bu in the *3*-position carried a high energy penalty of +11.5-15.2 kJmol^{-1}. Rotation of *t*Bu in the *5*-position had a low energy barrier with some dependence on the spin state: +0.3-0.5 kJmol^{-1} (Co(III)-cat) and +2.6-2.9 kJmol^{-1} (Co(II)-sq). An exception to the favoured *t*Bu orientations was the Co(III)-cat state of $[Co(Me_3tpa)(tBu_2diox)]^+$ which dissociated in *trans*-(b) geometry due to the steric hindrance of Me_3tpa at the Co(III) centre; however, the *trans*-(a) geometry remained intact. The crystal structures show some variation

from the most stable gas phase geometries but show the same orientation of the *t*Bu in the *3*-position (Figure S14).

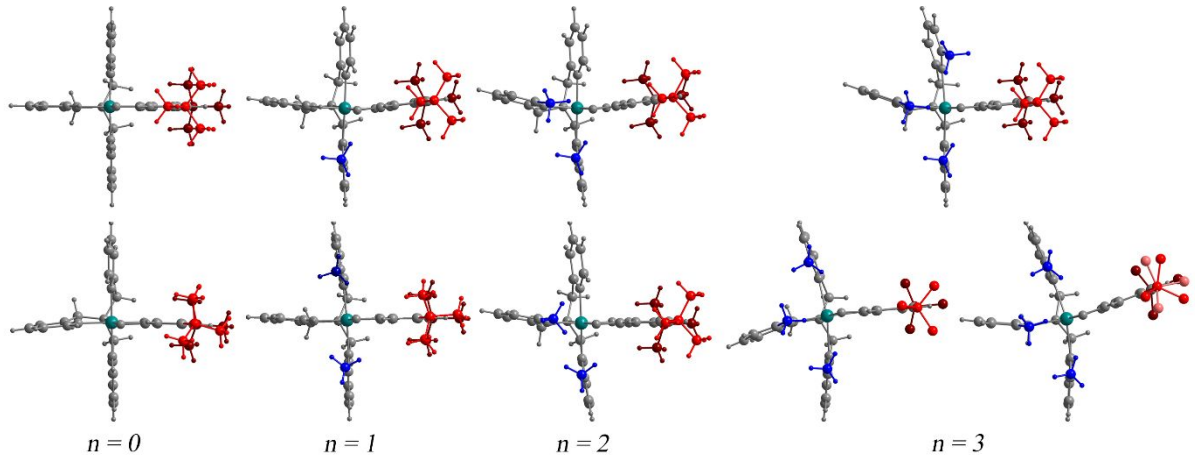

Figure S14. Comparison of DFT geometries with BP86/TZP theory (top row) with reported crystal structures (bottom row) for $[Co(Me_ntpa)(tBu_2diox)]^+$.[1] Colour code: Co, green; C, O and H, grey; tpa methyl group,: blue; disordered Me groups, dark blue; *t*Bu in 3-position, red; *t*Bu in 5-position, maroon; disordered *t*Bu in 3-position, pink.

The geometries of $[Co(Me_ntpa)(tBu_2diox)]^+$ (n = 1, 2) were determined assuming the most stable *ax* and *ax*-*eq* isomers (C_1 symmetry) and comparing the *trans*-(a) and *trans*-(b) orientations only. The *trans*-(b) orientation was the most stable for the two complexes in both spin states (see Table S9).

Table S9. Energies of geometry optimizations of $[Co(Me_ntpa)(tBu_2diox)]^+$ (n = 1, 2) with *t*Bu orientations as described in Figure S13 and BP86/TZP theory. Lowest energy isomers of each electromer are indicated in bold.

	Energy / kJ mol^{-1}			
	n = 1		***n = 2***	
Spin state	***trans*-(a)**	***trans*-(b)**	***trans*-(a)**	***trans*-(b)**
Co(III)-cat	-46883.54	**-46884.02**	-48444.76	**-48445.10**
Co(II)-sq	-46838.76	**-46841.44**	-48417.82	**-48420.55**

S.I.-8c Asymmetric Dioxolenes: Me_2diox

The lowest energy geometries of $[Co(Me_ntpa)(Me_2diox)]^+$ (n = 0-3) were identified, screening *(i)* the enforcement of C_S/C_1 symmetry, *(ii)* axial and equatorial isomers of n = 1, 2 complexes and *(iii)* the orientation of the methyl substituents on Me_2diox (see Table S10). From the optimizations outlined above the following assumptions were made: C_S geometries of Me_3tpa complexes were excluded; *cis* Me_2diox orientations were excluded; and only Me orientations in the equivalent of *trans*-(a) and *trans*-(b) positions were compared.

Calculations indicated that a bent C_1 geometry was favoured for all calculations, except for n = 0 in the Co(III)-cat spin state. The Metpa and Me_2tpa ligands adopted *ax* and *ax-eq* geometries, as favoured in H_4diox and Cl_4diox calculations. Orientation of methyl groups in the Me_2diox ligand favoured the *trans*-(b) geometry with the exception of $[Co(Me_ntpa)(Me_2diox)]^+$ (n = 0, 1) in the Co(III)-cat state which showed a slight preference (<0.3 kJmol^{-1}) for a different rotation of the *5*-position Me group. The lesser steric bulk of the Me group allowed the Me to rotate freely in most optimizations.

Table S10. Energies of geometry optimizations of $[Co(Me_ntpa)(Me_2diox)]^+$ with BP86/TZP theory. Lowest energy isomers of each electromer are indicated in bold.

n	Isomer	Me	Spin state	Energy / kJ mol^{-1}			Description
				C_S		C_1	
0	N/A	**(a)**	Co(III)-cat	**-35937.57**		-35937.42	planar
			Co(II)-sq	-35878.23		-35879.49	bent
		(b)	Co(III)-cat	-35937.29		-35937.37	planar
			Co(II)-sq	-35866.29		**-35880.82**	bent
				away	*towards*		
1	*eq*	**(a)**	Co(III)-cat	-37496.90	-37495.48	-37498.49	bent
			Co(II)-sq	-37444.60	-37452.65	-37458.27	bent
		(b)	Co(III)-cat	-37496.80	-37495.29	-37498.61	bent
			Co(II)-sq	-37446.57	-37446.49	-37458.27[b]	bent, *5*-Me down
	ax	**(a)**	Co(III)-cat	N/A		**-37507.10**[b]	bent, *5*-Me up
			Co(II)-sq			Moved[a]	N/A
		(b)	Co(III)-cat	N/A		-37507.02[b]	bent, *5*-Me up
			Co(II)-sq			**-37463.78**	bent
				away	*towards*		
2	*ax-ax*	**(a)**	Co(III)-cat	-39060.65	-39062.13	-39066.97[b]	planar, ring twisted, *5*-Me down
			Co(II)-sq	-39028.08	-39025.89	Moved[a]	N/A
		(b)	Co(III)-cat	-39060.33	-39061.84	-39067.61	planar, ring twisted
			Co(II)-sq	-39031.03	-39027.76	-39038.70	planar, ring twisted
	ax-eq	**(a)**	Co(III)-cat	N/A		-39068.13[b]	bent, *5*-Me up
			Co(II)-sq			Moved[a]	N/A
		(b)	Co(III)-cat	N/A		**-39068.24**	bent
			Co(II)-sq			**-39043.00**	bent
3	N/A	**(a)**	Co(III)-cat	Not considered		-40623.71	bent
			Co(II)-sq			Moved[a]	N/A
		(b)	Co(III)-cat	Not considered		**-40624.68**	bent
			Co(II)-sq			**-40617.17**	bent

[a] 5-Me group rotated to *trans*-(b) Me orientation, [b] *5*-Me group rotated

S.I.-9 DFT Calculations of Spin State Energies

Table S11. Absolute energies of [Co(Me_2tpa)(tBu$_2$diox)]$^+$ spin states using selected functionals and TZP/ZORA/COSMO method with DCM

Functional	Energy / kJ mol^{-1}	
	LS-Co(III)-cat	HS-Co(II)-sq
BP86	-48599.82	-48537.30
OPBE	-49149.56	-49141.41
B3LYP	-55804.05	-55836.34
B3LYP*	-53979.76	-53983.11
TPSSh	-54307.42	-54020.11

Table S12. Absolute energies of [Co(Me_ntpa)(Xdiox)]$^+$ family (n = 0-3) using the OPBE/TZP/ZORA/COSMO method with MeCN

	Energy LS-Co(III)-cat/ kJ mol^{-1}				Energy HS-Co(II)-sq/ kJ mol^{-1}			
X	n = 0	n = 1	n = 2	n = 3	n = 0	n = 1	n = 2	n = 3
tBu$_2$	-46018.84	-47589.93	-49149.56	-50706.65	-45966.91	-47556.82	-49141.41	-50723.78
Me$_2$	-36577.18	-38147.94	-39707.34	-41261.52	-36512.76	-38103.57	-39687.00	-41270.85
H$_4$	-33395.01	-34965.29	-36524.11	-38081.87	-33321.56	-34911.45	-36494.56	-38078.46
Cl$_4$	-32774.85	-34344.72	-35901.99	-37457.46	-32689.95	-34280.99	-35863.66	-37445.15
Br$_4$	-32527.33	-34096.23	-35654.39	-37208.59	-32438.87	-34030.11	-35608.80	-37196.92

Table S13. Absolute energies of selected [Co(Me_ntpa)(Xdiox)]$^+$ family (n = 2-3) using the OPBE/TZP/ZORA/COSMO method with DCM

Complex	Energy / kJ mol^{-1}	
	LS-Co(III)-cat	HS-Co(II)-sq
[Co(Me_2tpa)(tBu$_2$diox)]+	-49130.13	-49124.95
[Co(Me_3tpa)(Cl_4diox)]+	-37435.56	-37427.36
[Co(Me_3tpa)(Br_4diox)]+	-37185.88	-37178.83

S.I.-10 Spin Density Maps

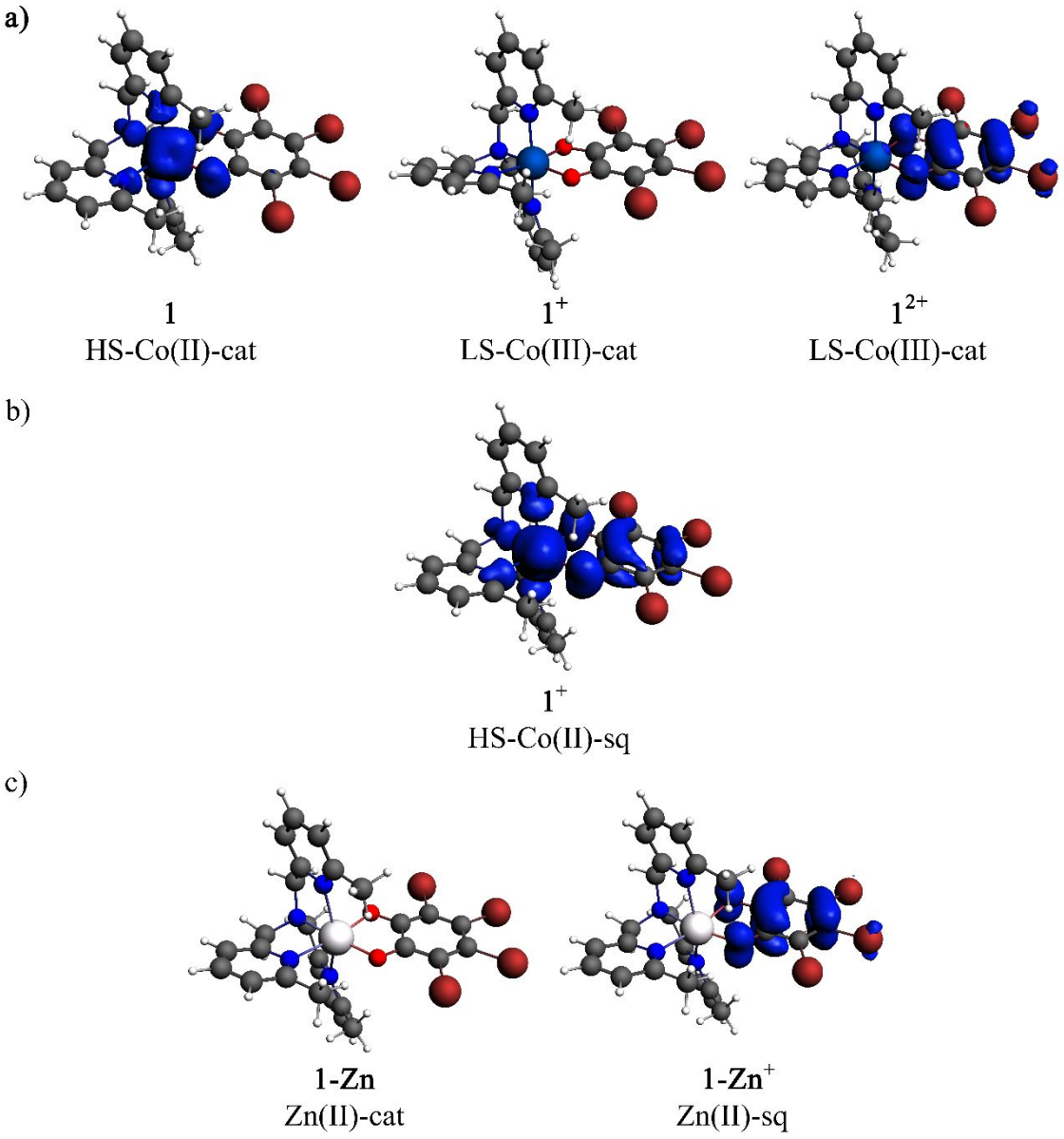

Figure S15. Spin density maps (blue) with a threshold value of 0.002 for a) the lowest energy electromers of **1** (quartet), $\mathbf{1}^{+}$ (singlet) and $\mathbf{1}^{2+}$ (doublet), b) the higher energy electromer of $\mathbf{1}^{+}$ (quintet) and c) the lowest energy electromers of **1-Zn** and **1-Zn**$^{+}$. Calculated with geometry optimization using the OPBE/TZP/ZORA/COSMO method with DMF as the solvent.

References

1. Beni, A.; Dei, A.; Laschi, S.; Rizzitano, M.; Sorace, L., Tuning the charge distribution and photoswitchable properties of cobalt-dioxolene complexes by using molecular technique. *Chem. - Eur. J.* **2008**, *14*, 1804-1813.

2. Dei, A., Correlations between optical charge transfer energies and electrochemical data: the iron(III)-catecholato system. *Inorg. Chem.* **1993**, *32*, 5730-5733.

3. Benelli, C.; Dei, A.; Gatteschi, D.; Pardi, L., Redox potentials and charge transfer spectra of catecholate and semiquinone adducts of a cobalt-tetraazamacrocyclic complex. *Inorg. Chim. Acta* **1989**, *163*, 99-104.

4. Bencini, A.; Caneschi, A.; Carbonera, C.; Dei, A.; Gatteschi, D.; Righini, R.; Sangregorio, C.; van Slageren, J., Tuning the physical properties of a metal complex by molecular techniques: the design and the synthesis of the simplest cobalt-*o*-dioxolene complex undergoing valence tautomerism. *J. Mol. Struct.* **2003**, *656*, 141-154.

5. Becke, A. D., Density-functional exchange-energy approximation with correct asymptotic behavior. *Phys. Rev. A* **1988**, *38*, 3098-3100.

6. Perdew, J. P., Density-functional approximation for the correlation energy of the inhomogeneous electron gas. *Phys. Rev. B* **1986**, *33*, 8822-8824.

7. Cheyne, S. E.; McClintock, L. F.; Blackman, A. G., Stabilization of Coordinated Carbonate in Aqueous Acidic Solution: Steric Inhibition of Protonation in Co(III) Complexes Containing Chelated Carbonate. *Inorg. Chem.* **2006**, *45*, 2610-2618.

8. McClintock, L. F.; Cavigliasso, G.; Stranger, R.; Blackman, A. G., The donor ability of the chelated carbonate ligand: protonation and metalation of $[(L)Co(O_2CO)]^+$ complexes in aqueous solution. *Dalton Trans.* **2008**, 4984-4992.

9. Mulyana, Y.; Alley, K. G.; Davies, K. M.; Abrahams, B. F.; Moubaraki, B.; Murray, K. S.; Boskovic, C., Dinuclear cobalt(II) and cobalt(III) complexes of bis-bidentate naphthoquinone ligands. *Dalton Trans.* **2014**, *43*, 2499-2511.

10. Dapporto, P.; Dei, A.; Poneti, G.; Sorace, L., Complete direct and reverse optically induced valence tautomeric interconversion in a cobalt-dioxolene complex. *Chem. - Eur. J.* **2008**, *14*, 10915-10918.

11. Cho, J.; Furutachi, H.; Fujinami, S.; Suzuki, M., A Bis(μ-alkylperoxo)dinickel(II) Complex as a Reaction Intermediate for the Oxidation of the Methyl Groups of the Me_2-tpa Ligand to Carboxylate and Alkoxide Ligands. *Angew. Chem. Int. Ed.* **2004**, *43*, 3300-3303.

12. Cho, J.; Furutachi, H.; Fujinami, S.; Tosha, T.; Ohtsu, H.; Ikeda, O.; Suzuki, A.; Nomura, M.; Uruga, T.; Tanida, H.; Kawai, T.; Tanaka, K.; Kitagawa, T.; Suzuki, M., Sequential Reaction Intermediates in Aliphatic C−H Bond Functionalization Initiated by a Bis(μ-oxo)dinickel(III) Complex. *Inorg. Chem.* **2006**, *45*, 2873-2885.

13. Matsumoto, T.; Nagahama, T.; Cho, J.; Hizume, T.; Suzuki, M.; Ogo, S., Preparation and Reactivity of a Nickel Dihydride Complex. *Angew. Chem. Int. Ed.* **2011**, *50*, 10578-10580.

14. Benhamou, L.; Lachkar, M.; Mandon, D.; Welter, R., The preparation and full characterization of dichloroferrous complexes of mono-, bis- and tris-α-methyl substituted tris(2-pyridylmethyl)amine (TPA) ligands. Structural bases of stability of the complexes in solution. *Dalton Trans.* **2008**, 6996-7003.

15. Shiren, K.; Fujinami, S.; Suzuki, M.; Uehara, A., Synthesis, Structures, and Magnetic Properties of Heterodimetal Bis(μ-hydroxo)chromium(III)nickel(II) Complexes with Tpa Derivatives Having Sterically Bulky Substituents. *Inorg. Chem.* **2002**, *41*, 1598-1605.

16. Goodson, P. A.; Oki, A. R.; Glerup, J.; Hodgson, D. J., Design, synthesis, and characterization of bis(*μ*-oxo)dimanganese(III,III) complexes. Steric and electronic control of redox potentials. *J. Am. Chem. Soc.* **1990**, *112*, 6248-6254.

17. Goodson, P. A.; Oki, A. R.; Hodgson, D. J., Monomeric complexes of manganese(II) with tetradentate ligands: isolation of *cis*-diaquamanganese(II) and *cis*-dichloromanganese(II) species. *Inorg. Chim. Acta* **1990**, *177*, 59-64.

18. Boldog, I.; Muñoz-Lara, F. J.; Gaspar, A. B.; Muñoz, M. C.; Seredyuk, M.; Real, J. A., Polynuclear Spin Crossover Complexes: Synthesis, Structure, and Magnetic Behavior of $[Fe_4(\mu\text{-}CN)_4(phen)_4(L)_2)]^{4+}$ Squares. *Inorg. Chem.* **2009**, *48*, 3710-3719.

19. Hayashi, H.; Fujinami, S.; Nagatomo, S.; Ogo, S.; Suzuki, M.; Uehara, A.; Watanabe, Y.; Kitagawa, T., A Bis(*μ*-oxo)dicopper(III) Complex with Aromatic Nitrogen Donors: Structural Characterization and Reversible Conversion between Copper(I) and Bis(*μ*-oxo)dicopper(III) Species. *J. Am. Chem. Soc.* **2000**, *122*, 2124-2125.

20. Horner, L.; Geyer, E., Zur Kenntnis der o-Chinone, XXVII: Redoxpotentiale von Brenzcatechin-Derivaten. *Chem. Ber.* **1965**, *98*, 2016-2045.